A Photonic Topological Mode Bound to a Vortex

Adrian J Menssen,[1,*] Jun Guan,[2,†] David Felce,[1] Martin J Booth,[2] and Ian A Walmsley[1,3]

[1] *University of Oxford, United Kingdom, Department of Atomic and Laser Physics*
[2] *University of Oxford, United Kingdom, Department of Engineering Science*
[3] *Imperial College London, United Kingdom*

(Dated: June 29, 2020)

We report the observation of a mode associated with a topological defect in the bulk of a 2D photonic material by introducing a vortex distortion to an hexagonal lattice analogous to graphene. The observed modes lie mid-gap at zero energy and are closely related to Majorana bound states in superconducting vortices. This is the first experimental demonstration of the Jackiw-Rossi model [R. Jackiw and P. Rossi, Nuclear Physics B 190, 681 (1981)].

PACS numbers: 03.75.Lm, 42.82.Et

I. INTRODUCTION

Phenomena associated with the topological characteristics of physical systems are of wide-reaching interest in many fields in physics, with applications ranging from condensed matter physics [1–3] to particle physics [4, 5] and cosmology [6]. Most prominently topology has been applied in condensed matter physics, where the importance of the topology of the band structure was first recognised in the discovery of the integer quantum Hall effect [7]. Subsequently many classes of topological insulators and superconductors have been discovered [2]. A key characteristic of a system with non-trivial topology is the presence of topological invariants, integer numbers that classify the topological structure. They are preserved under smooth, 'homotopic' deformations of the Hamiltonian. At the boundary between domains governed by different such invariants, where the topology abruptly changes, a topological defect occurs. Localised at these defects are states protected by the topology of the system: they are robust to errors in the underlying Hamiltonian. These 'edge states' have been investigated extensively in photonic platforms [8–12]. Their study generated important insight into the physics of topological insulators [10] and spawned technological advances such as the development of topological lasers [13], where lasing occurs in edge states, protected from imperfections. Here, in contrast, we investigate for the first time a state bound to a vortex, a point defect, in the bulk of a 2D photonic material (photonic graphene). These modes are 'zero modes', as they lie mid-gap, at zero energy. The vortex-bound zero modes we consider here are of significant interest to solid-state physics. In topological superconductors they support Majorana bound states at the vortex core [2, 14–16]. The vortex defect we realise here are photonic analogues of the vortices in topological superconductors explored by Reed, Green [16] and Volovik [15]. Majorana bound states at these vortices are a promising candidate for the realisation of a topological quantum computer [17]. The Jackiw-Rossi [5] model was originally introduced in a quantum field theory context to describe fermions in a 2+1D system coupled to a complex scalar field in the Dirac equation. Jackiw and Rossi [5] demonstrated that if the scalar field contains a vortex it supports localised zero-energy solutions at the vortex core. Witten [6] also considered the Jackiw-Rossi type vortex defect in the context of superconducting cosmic strings.

Particles in a tight binding model of graphene can be shown to obey a Dirac equation near the 'Dirac' cones in the band structure. Hou, Chamon and Mudry [18] predicted zero modes in graphene which realise the Jackiw-Rossi model: Small perturbations to the graphene lattice induce the scalar-field coupling to the effective Dirac equation governing the graphene tight binding model. A photonic platform allows for a high degree of control over the system parameters and is thus a powerful tool to investigate topological effects, where in solid state systems this degree of control is notoriously difficult to engineer. The vortex topological defect is realised by introducing a distortion to the waveguide position in a hexagonal waveguide lattice as was suggested by Iadecola et. al. [19]. We show adiabatic transport of the zero mode as the vortex is moved, as well as topological protection against imperfections of the waveguide lattice.

II. THEORY

The wavefunction evolution generated by a tight binding Hamiltonian can be mapped directly to the coupled mode equations of light propagating through a photonic crystal, where the time dimension in the Schrödinger equation takes the role of the propagation direction of the light through the crystal:

$$i\frac{\partial\psi_{\mathbf{r}}(z)}{\partial z} = \sum_{j=1}^{3} H_{\mathbf{r},\mathbf{r}+\mathbf{s_j}}\psi_{\mathbf{r}\pm\mathbf{s_j}}(z) \tag{1}$$

$\psi_{\mathbf{r}}(z)$ is the electric field amplitude at lattice site $\mathbf{r}$ and z is the length of the crystal the light has propagated

* adrian.menssen@physics.ox.ac.uk
† jun.guan@eng.ox.ac.uk

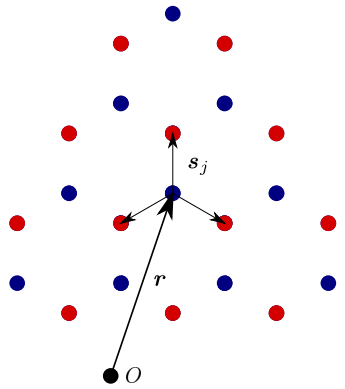

FIG. 1. Hexagonal lattice with two triangular sublattices (A and B) in red and blue, lattice vector $\mathbf{r}$ and vectors between nearest neighbours $\mathbf{s_j}$ indicated.

through, $\mathbf{s_j}$ points to its jth nearest neighbour (see Fig. 1). The complex scalar field $\Delta(\mathbf{r})$ containing the vortex can be simulated by introducing a distortion $\delta_{\mathbf{r},\mathbf{s_j}}$ to the nearest neighbour hopping strength t of graphene [18]:

$$\begin{aligned} H_{\mathbf{r},\mathbf{r}+\mathbf{s_j}} &= -t - \delta_{\mathbf{r},\mathbf{s_j}} \\ \delta_{\mathbf{r},\mathbf{s_j}} &= \frac{1}{2}\Delta(\mathbf{r}) e^{i\mathbf{K}_+\mathbf{s_j}} e^{i\mathbf{2}i\mathbf{K}_+\mathbf{r}} + c.c., \end{aligned} \tag{2}$$

$\mathbf{K}_+ = (4\pi/(3\sqrt{3}a), 0)$ marks the position of Dirac point in the reciprocal lattice. a is the lattice constant. The explicit form of $\Delta(\mathbf{r})$ containing a vortex at $\mathbf{r} = 0$ is:

$$\begin{aligned} \Delta(\mathbf{r}) &= \Delta_0(r) e^{i(\alpha + N\phi)} \\ \Delta_0(r) &= \Delta_0 \tanh(r/l_0), \end{aligned} \tag{3}$$

where ϕ is the polar angle of $\mathbf{r}$, l_0 the width of the vortex, α the phase of the vortex and N the vorticity, the topological invariant of the system. The sign of the vorticity determines which of the two triangular sublattices of graphene (see Fig. 1) supports the mode (1 for sublattice A, -1 for sublattice B). In this work we set its value to 1: the mode is confined to sublattice A, whereas the distortion is applied to sublattice B. For the vortex phase we chose $\alpha = \pi/2$. The radial dependence of the zero mode-wavefunction $\phi_A(r)$ localised on sublattice A (a solution to the mode-coupling equations (1)) is given by [15, 18, 20]:

$$\phi_A(r) \sim e^{i(-\frac{\alpha}{2}+\frac{\pi}{4})} e^{-\int_0^r \mathrm{d}r' \Delta_0(r')}. \tag{4}$$

The electrical field strength is given by:

$$E(\mathbf{r}, z, t) \sim \mathrm{Re}[(\phi_A(r) e^{i\mathbf{K}_+\mathbf{r}} + c.c.) e^{ik_\omega z - i\omega t}], \tag{5}$$

where $\mathbf{r}$ points to a lattice site on the supporting sublattice A. The vortex in $\Delta(\mathbf{r})$ and the zero-mode state bound to it are visualised in Fig. 2 a). The distortions $\delta_{\mathbf{r},\mathbf{s_j}}$ of the coupling Hamiltonian are implemented with small shifts in the wave-guides' positions (illustrated in Fig. 2 b)), assuming exponential decay of the field away from the waveguides. The exponential decay was measured experimentally for different waveguide positions and relative orientations (see Supplementary IV [21]). We note that it is the collective effect of small distortions applied to every lattice site which gives rise to the topologically confined mode at the centre of the vortex defect.

III. EXPERIMENTAL RESULTS

A. Excitation of the vortex mode

First, we demonstrate a stationary photonic bulk zero-mode. The vortex distortion is located at the centre of the lattice, as shown in Fig. 2a/b). In Fig. 2c), comparing the experimental result (top) and the theoretical calculation (bottom), we see that they match very well. The waveguide mode intensity pattern is governed by equations (4) and (5). The mode is excited using 7 individual phase and amplitude tuned beams directed at waveguides on sublattice A carrying the majority of the mode (Fig. 2 d). We use a gradient descent algorithm to optimise the phases and amplitudes for maximum overlap with the zero mode (see Supplementary II). The light in the zero mode is tightly confined to the centre of the vortex and decays quickly outside the radius of the vortex $l_0 = 20\ \mu m$, with a decay length governed by equation (4). Most of the intensity is confined to the sublattice which carries the bulk zero-mode, as designed. Residual background originates from imperfect overlap of the exciting light field with the zero mode. Other imperfections arise from residual next-nearest neighbour coupling (see Supplementary V). We estimate the ratio of nearest to next nearest neighbour coupling strength to be less than 5%. To quantify the degree to which this intensity pattern represents the zero-mode, we introduce the ratio of light intensity between the two sublattices:

$$\gamma_{AB} = \frac{\text{Light intensity in sublattice A}}{\text{Light intensity in sublattice B}} \tag{6}$$

as a measure of fidelity for the excitation of the mode, should be confined to one sublattice only. For a mode confined to sublattice A, we expect $\gamma_{AB} \gg 1$. The measured mode displayed in the top panel of Fig. 2 c) has $\gamma_{AB} = 4.8$. To ensure we only consider contributions from the zero mode, we integrate the light intensity within a 30 μm radius around the vortex centre.

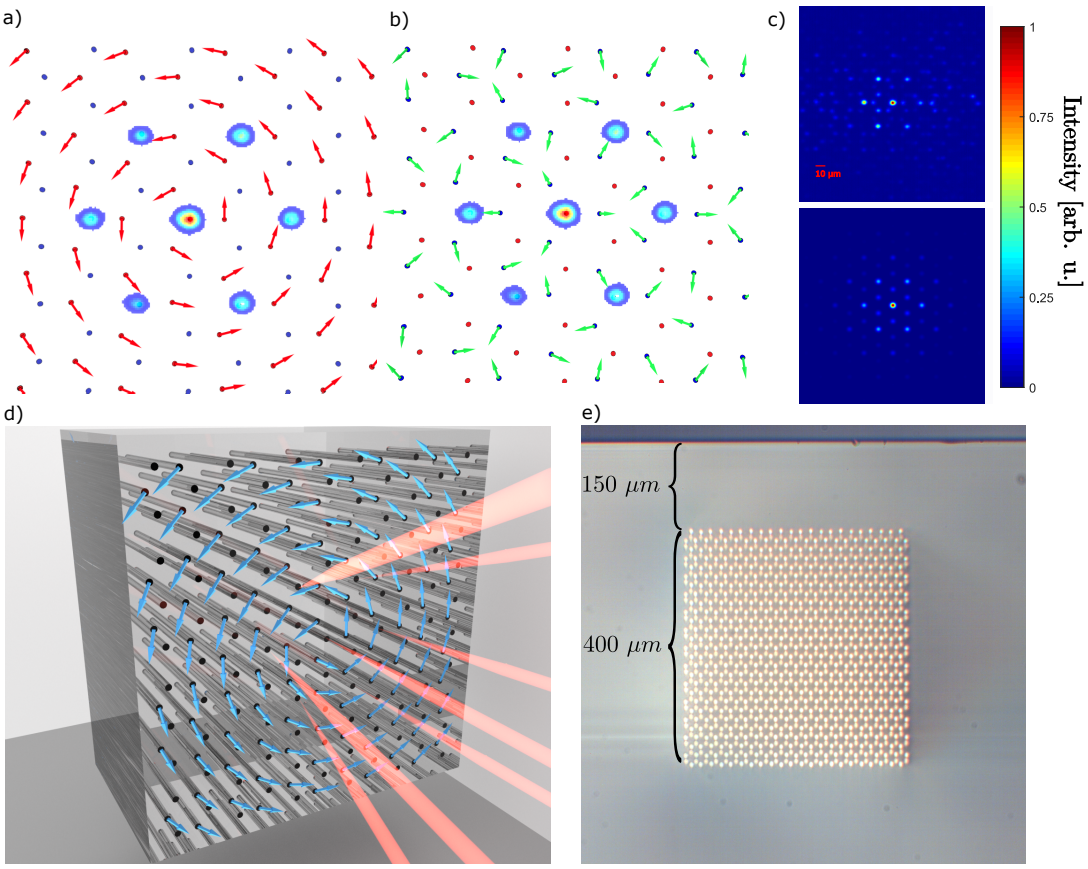

FIG. 2. a) Photonic lattice with $\Delta(\mathbf{r})$ represented by red arrows. Bulk zero-mode intensity for dominant modes indicated at the centre of the vortex. For visualising the order parameter, the complex function $\Delta(\mathbf{r})$ is mapped onto a vector field through the correspondence $\mathbb{C} \rightarrow (\mathrm{Re}[\Delta(\mathbf{r})], \mathrm{Im}[\Delta(\mathbf{r})])$. b) Shift of the waveguide positions from the graphene lattice configuration, which implements the topological vortex distortion, indicated by green arrows. c) Comparison between the camera image of an observed stationary topological bulk zero mode (Top) and the theoretical model (Bottom). The theory has been convolved a with a Gaussian to approximate the modes of the waveguides. d) Illustration of multi-beam excitation of the photonic lattice. An array of phase and amplitude tuned beams directed at individual waveguides carrying the majority of the intensity is used to achieve coherent excitation of the zero mode in the centre of the vortex. e) Image of the end-facet of the silica chip, showing the full lattice of 1192 waveguides.

B. Adiabatic translation of the zero mode

Next, we translate the vortex zero mode transversely across the waveguide lattice by adiabatically shifting the vortex from one side of the lattice to the other by around 100 μm. In the experiment, a 9 cm long chip is used to ensure adiabatic translation of the zero mode. We can observe transverse translation of the zero-mode with most of the transmitted intensity confined around the centre of the shifted vortex and in the correct sublattice (with a ratio of $\gamma_{AB} = 4.7$, Fig. 3 a), top panel). The measured mode is no longer symmetrical, likely due to small variations in waveguide lattice fabrication which can easily shift the relative intensities within waveguides in the zero mode. In the bottom panel of Fig. 3 a), we show what happens if we try to excite the mode at a position in the lattice where there is no vortex present. As expected, we are not able to excite a mode and see no light transport. The ratio of intensities is: $\gamma_{AB} = 0.67$.

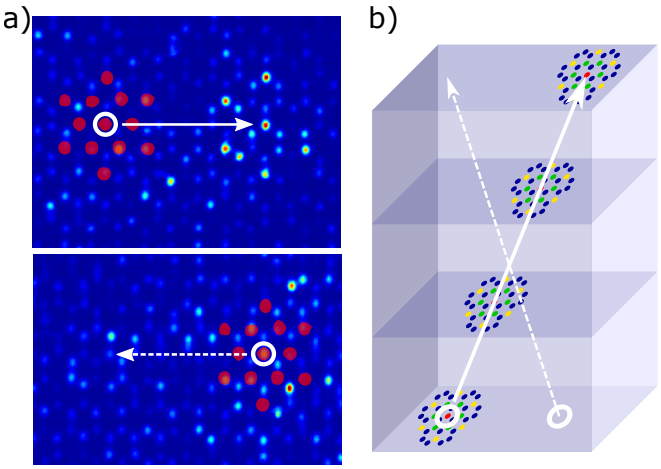

FIG. 3. a) Top panel: Recorded bulk zero-mode transverse translation, in which the zero-mode is translated from left (at input side schematically shown in b)) to right (at the output side) of the lattice. Red dots indicate the positions of the 13 beams used to excite the zero mode at the input. The circled waveguide marks the position of the centre at the input side. $\gamma_{AB} = 4.7$. Bottom panel: the same number of waveguides are excited on the input side of the lattice, where no vortex is present. At output side, $\gamma_{AB} = 0.67$. Also, the total light intensity in the displayed region is substantially less as most of the light is scattered into the rest of the lattice. The colour scale is normalised to the brightest peak in both pictures. b) Illustration of mode shifting by adiabatically translating (solid arrow) the centre of the vortex (dotted pattern) along the longitudinal direction of waveguide lattice; the dashed arrow indicates the direction the vortex moves in.

C. Topological protection

To demonstrate that the zero-mode is topologically protected against random errors of the lattice, we deliberately introduce an error to the position of the waveguides by shifting them by a random distance, sampled from a two-dimensional uniform distribution, where the radius r_d of the distribution corresponds to the maximum shift applied. We note that our mode is protected against any error which preserves chiral symmetry, such as random errors in wave guide position. In Fig. 4, we show the recoded zero-modes at four different distortion levels with $r_d = 0, 200, 400, 600$ nm respectively. The systematic topological distortion, which is introduced to the hexagonal lattice for the formation of the vortex, is approximately 850 nm. We can observe that the zero-mode remains visible even when large random errors in waveguide position are introduced. The larger the error distortion, the more light leaks into the other sublattice. We measure a steadily decreasing amount of light in the correct sublattice $\gamma_{AB} = 3.8, 2.9, 2.2, 2.1$ as the error distortion increases.

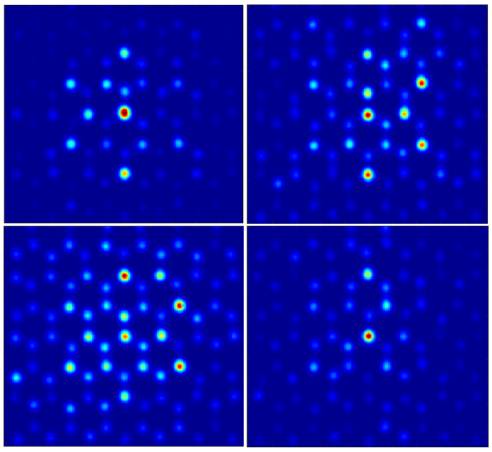

FIG. 4. Topological mode with random error distortions. Top left: no error, Top right: maximum 200 nm, Bottom left: maximum 400 nm, Bottom right: maximum 600 nm. The ratios of light intensity in the zero-mode sublattice to the non-mode supporting one are $\gamma_{AB} = 3.8, 2.9, 2.2, 2.1$ respectively. The colour map of each image is normalised independently.

IV. METHODS

Waveguide lattice: Our photonic crystal lattices are fabricated in glass through femtosecond laser direct writing [22] (see also Supplementary III)). By employing advanced aberration correction techniques [23], we are able to write waveguide lattices of good homogeneity in depths of up to 1 mm. The dimension of the waveguide lattice is around 400x400 μm. Each waveguide lattice consists of 1192 waveguides that are arranged to form a hexagonal lattice. The distance between lattice sites is around 10 μm. Mode excitation scheme: To excite the bulk zero mode, we developed a method based on an SLM to simultaneously illuminate multiple waveguides with beams of individually controlled phase and amplitude, as illustrated in Fig. 2 d). As coherent light source we use

a laser diode at 785 nm. Multiple beams (up to 13 in the present work) are directed at individual waveguides near the centre of the vortex. Phases and amplitudes of all beams are tuned to excite the zero mode (setup described in Supplementary I).

V. ACKNOWLEDGEMENTS

We especially want to thank for their constructive input Claudio Chamon, Tom Iadecola and Thomas Schuster. We thank Bryn Bell for sharing his knowledge in topological photonics. Furthermore, we would like to acknowledge Steve Simon and Glenn Wagner for providing valuable insights into solid state theory, Helen Chrzanowski for her experimental expertise and Steve Kolthammer for initial discussions. We thank Patrick Salter for sharing his expertise in aberration correction techniques. AJM is supported by the Buckee Scholarship at Merton College. This work was funded by the EPSRC through the Programme Grant EP/K034480/1, and by the European Union through the ERC Advanced Grant MOQUACINO.

VI. AUTHOR CONTRIBUTIONS

AJM conducted the theoretical simulations, conceived the idea for the SLM based method of exciting multiple waveguides and wrote the paper with input from the other authors. JG built the adaptive femtosecond laser writing system, implemented the adaptive aberration correction and fabricated the chips. AJM and DF built and conducted the experiment. DF worked on the development and implementation of the method to control phase and amplitude of the light field. IAW, AJM, JG and MJB conceived the project. IAW and MJB supervised the project.

VII. CONCLUSION

We have demonstrated for the first time an experimental implementation of the Jackiw-Rossi model and observed the characteristic topological vortex zero mode in a photonic lattice. We excited the spatially delocalised mode at multiple sites, enabling us to resolve its structure. We showed that the mode can be adiabatically shifted across the photonic lattice and that it is topologically protected. Possible applications of these modes may lie in the protection of information encoded in quantum states against inevitable fabrication errors [11, 24] in linear optical circuits by injecting multiple entangled particles into different protected vortex modes. Further, the degree of control we have demonstrated over these localised, protected topological bulk zero-modes may in the future enable applications probing the effects under exchange of multiple zero modes, as was suggested by Iadecola et. al. [19]. These modes will accumulate a geometric phase when two of them are "braided" around each other. Following our work, Noh et. al. [25] have recently explored this type of defect, suggesting a geometric phase may be observed in a system consisting of a stationary, strongly localised defect mode and a simulated second defect. Moreover, our demonstration also provides the possibility for further studying models employed in high energy physics, as well as new implementations of topological lasers other than those which have already been demonstrated in edge-states [13, 26]. Recently, X. Gao et. al. [27] have implemented a Jackiw-Rossi type defect in an optical micro cavity using a Silicon On Oxide (SOI) platform. The authors envisage applications for Vertical-Cavity Surface-Emitting Lasers (VCSEL) that use this mode for stable lasing. The topic of topological vortex defects has also recently been explored in other platforms: P. Gao et. al. [28] realised a topological vortex defect in a sonic lattice. Chen et. al. [29] have studied a mechanical analogue of the Jackiw-Rossi mode.

[1] M. Z. Hasan and C. L. Kane, Reviews of modern physics **82**, 3045 (2010).
[2] J. C. Y. Teo and C. L. Kane, Physical Review B **82**, 115120 (2010).
[3] X.-L. Qi and S.-C. Zhang, Rev. Mod. Phys. **83**, 1057 (2011).
[4] R. Jackiw and C. Rebbi, Physical Review D **13**, 3398 (1976).
[5] R. Jackiw and P. Rossi, Nuclear Physics B **190**, 681 (1981).
[6] E. Witten, Nuclear Physics B **249**, 557 (1985).
[7] D. J. Thouless, M. Kohmoto, M. P. Nightingale, and M. den Nijs, Phys. Rev. Lett. **49**, 405 (1982).
[8] M. C. Rechtsman, Y. Plotnik, J. M. Zeuner, D. Song, Z. Chen, A. Szameit, and M. Segev, Physical review letters **111**, 103901 (2013).
[9] Y. Plotnik, M. C. Rechtsman, D. Song, M. Heinrich, J. M. Zeuner, S. Nolte, Y. Lumer, N. Malkova, J. Xu, A. Szameit, and Others, Nature materials **13**, 57 (2014).
[10] S. Stützer, Y. Plotnik, Y. Lumer, P. Titum, N. H. Lindner, M. Segev, M. C. Rechtsman, and A. Szameit, Nature **560**, 461 (2018).

[11] J. Noh, W. A. Benalcazar, S. Huang, M. J. Collins, K. P. Chen, T. L. Hughes, and M. C. Rechtsman, Nature Photonics , 1 (2018).

[12] M. Hafezi, S. Mittal, J. Fan, A. Migdall, and J. M. Taylor, Nature Photonics **7**, 1001 (2013).

[13] M. A. Bandres, S. Wittek, G. Harari, M. Parto, J. Ren, M. Segev, D. N. Christodoulides, and M. Khajavikhan, Science **359**, eaar4005 (2018).

[14] C. Chamon, C.-y. Hou, C. Mudry, and S. Ryu, (2012), 10.1088/0031-8949/2012/T146/014013.

[15] G. E. Volovik, Journal of Experimental and Theoretical Physics Letters **70**, 609 (1999).

[16] N. Read and D. Green, Phys. Rev. B **61**, 10267 (2000).

[17] C. Nayak, S. H. Simon, A. Stern, M. Freedman, and S. D. Sarma, Reviews of Modern Physics **80**, 1083 (2008).

[18] C.-Y. Y. Hou, C. Chamon, and C. Mudry, Physical review letters **98**, 186809 (2007), arXiv:0609740 [cond-mat].

[19] T. Iadecola, T. Schuster, and C. Chamon, Physical review letters **117**, 73901 (2016).

[20] R. Jackiw and S. Y. Pi, Physical Review Letters **98**, 1 (2007), arXiv:0701760 [cond-mat].

[21] A detailed description our experimental methods can be found in the Supplementary [url] which includes Refs. [30–37].

[22] A. Szameit and S. Nolte, Journal of Physics B: Atomic, Molecular and Optical Physics **43**, 163001 (2010).

[23] L. Huang, P. S. Salter, F. Payne, and M. J. Booth, Optics Express **24**, 10565 (2016).

[24] M. C. Rechtsman, Y. Lumer, Y. Plotnik, A. Perez-Leija, A. Szameit, and M. Segev, Optica **3**, 925 (2016).

[25] J. Noh, T. Schuster, T. Iadecola, S. Huang, M. Wang, K. P. Chen, C. Chamon, and M. C. Rechtsman, arXiv preprint arXiv:1907.03208 (2019).

[26] S. Mittal, E. A. Goldschmidt, and M. Hafezi, Nature , 1 (2018).

[27] X. Gao, L. Yang, H. Lin, L. Zhang, J. Li, F. Bo, Z. Wang, and L. Lu, arXiv preprint arXiv:1911.09540 (2019).

[28] P. Gao, D. Torrent, F. Cervera, P. San-Jose, J. Sánchez-Dehesa, and J. Christensen, Physical review letters **123**, 196601 (2019).

[29] C.-W. Chen, N. Lera, R. Chaunsali, D. Torrent, J. V. Alvarez, J. Yang, P. San-Jose, and J. Christensen, Advanced Materials **31**, 1904386 (2019).

[30] T.-L. Kelly and J. Munch, Appl. Opt. **37**, 5184 (1998).

[31] L. G. Neto, D. Roberge, and Y. Sheng, Appl. Opt. **35**, 4567 (1996).

[32] R. Dou and M. K. Giles, Appl. Opt. **35**, 3647 (1996).

[33] S. Chavali, P. M. Birch, R. Young, and C. Chatwin, Optics and Lasers in Engineering **45**, 413 (2007).

[34] V. Bagnoud and J. D. Zuegel, Opt. Lett. **29**, 295 (2004).

[35] V. Arrizón, Opt. Lett. **28**, 1359 (2003).

[36] S. A. Goorden, J. Bertolotti, and A. P. Mosk, Optics Express **22**, 17999 (2014), arXiv:1405.3893.

[37] P. S. Salter, M. Baum, I. Alexeev, M. Schmidt, and M. J. Booth, Opt. Express **22**, 17644 (2014).